Int J Earth Sci (Geol Rundsch) (2017) 106:1375–1389
DOI 10.1007/s00531-016-1338-8

ORIGINAL PAPER

Zircon U–Pb geochronology, and elemental and Sr–Nd–Hf–O isotopic geochemistry of post-collisional rhyolite in the Chiang Khong area, NW Thailand and implications for the melting of juvenile crust

Xin Qian[1,2] · Yuejun Wang[1,3] · Qinglai Feng[2] · Jian-Wei Zi[4] · Yuzhi Zhang[1] · Chongpan Chonglakmani[5]

Received: 21 December 2015 / Accepted: 4 May 2016 / Published online: 4 June 2016

Abstract Volcanic rocks are widely exposed within the Chiang Khong–Lampang–Tak igneous zone in NW Thailand. A representative rhyolite sample from the Chiang Khong area yielded a zircon U–Pb age of 230.7 ± 1.1 Ma (n = 20, MSWD = 0.98). The Chiang Khong rhyolites are characterized by low TiO_2 (0.29–0.62 wt%) and MgO (0.04–0.82 wt%) with A/CNK values of 0.95–1.06 (one outlier at 1.47), and can be classified as highly fractionated I-type rhyolites. They are enriched in LILEs and LREEs, and depleted in HFSEs. Two representative samples have $^{87}Sr/^{86}Sr$ (i) ratios of 0.70497 and 0.70527, and the ε_{Nd} (t) values fall at +1.1 and +1.3, respectively. ε_{Hf} (t) and $\delta^{18}O$ in zircon are between +4.7 to +12.0 and 5.3 to 5.9 ‰, respectively. Our geochemical data suggest that the Chiang Khong rhyolites formed by partial melting of juvenile mafic lower crust in a post-collisional setting. Deep crustal anatexis was probably induced by upwelling asthenospheric mantle, shortly after slab detachment subsequent to closure of the Paleo-Tethys.

✉ Yuejun Wang
wangyuejun@mail.sysu.edu.cn

1 School of Earth Science and Geological Engineering, Sun Yat–Sen University, No. 135, Xingang Xi Road, Guangzhou 510275, People's Republic of China

2 State Key Laboratory of Geological Processes and Mineral Resources, Faculty of Earth Sciences, China University of Geosciences, Wuhan 430074, People's Republic of China

3 CAS Center for Excellence in Tibetan Plateau Earth Sciences, Chinese Academy of Sciences, Beijing 100101, People's Republic of China

4 Department of Applied Geology, Curtin University, Perth, WA 6102, Australia

5 School of Geotechnology, Suranaree University of Technology, Nakhon Ratchasima 30000, Thailand

Keywords Post-collisional rhyolite · Zircon U–Pb geochronology · Sr–Nd–Hf–O isotopic composition · Melting of juvenile mafic lower crust · Late Triassic · NW Thailand

Introduction

Western Yunnan and its southern extension (e.g., NW Laos and NW Thailand) are key areas for investigating and understanding the Paleo-Tethys tectonic evolution (Fig. 1a). In these areas, there developed several important suture zones including the Jinshajiang–Ailaoshan and Changning–Menglian suture zones in SW China, the Chiang Mai and Nan suture zones and the Loei tectonic zone in NW Thailand, and the Luang Prabang tectonic zone in NW Laos (Liu et al. 1991; Intasopa and Dunn 1994; Leloup et al. 1995; Wu et al. 1995; Mo et al. 1998; Zhong 1998; Ueno and Hisada 2001; Feng et al. 2005; Panjasawatwong et al. 2006; Sone and Metcalfe 2008; Sone et al. 2012; Zi et al. 2012, 2013; Qian et al. 2015, 2016a). Besides, two giant igneous zones, the Lancangjiang zone in SW Yunnan and the Chiang Khong–Lampang–Tak zone in NW Thailand, have been identified (Fig. 1a; e.g., Barr et al. 2000, 2006; Panjasawatwong 2003; Peng et al. 2006, 2008, 2013; Srichan et al. 2009; Wang et al. 2010; Barr and Charusiri 2011; Qian et al. 2013, 2016b). Along the Lancangjiang igneous zone, previous works on the metamorphic and magmatic rocks have revealed tectonic processes involving Permian eastward subduction of the Paleo-Tethys Ocean and subsequent Triassic collisional orogeny (Mo et al. 1998; Zhong 1998; Metcalfe 2002; Peng et al. 2006, 2008, 2013; Hennig et al. 2009; Wang et al. 2010; Dong et al. 2013; Fan et al. 2015). The Chiang Khong–Lampang–Tak igneous zone between the Chiang Mai and Nan suture

zones is a segment of a huge igneous belt. Recent studies have suggested that it can link with the Lancangjiang igneous zone to the north (Fig. 1a; Barr et al. 2000, 2006; Panjasawatwong 2003; Barr and Charusiri 2011; Qian et al. 2013, 2016b). The abundant Permian–Triassic volcanic rocks in the zone are characterized by a mafic–intermediate–felsic association. Existing studies have been focused on the general lithofacies and lithochemical characters of regional stratigraphy, however, the petrogenesis and tectonic implications of the Late Triassic felsic rocks remain poorly understood. Our recent investigations have newly identified a Late Triassic I-type rhyolite in the Chiang Khong area, northern part of the Chiang Khong–Lampang–Tak igneous zone. In this paper, we present new geochronological, geochemical results and zircon Hf and O isotopic data for the Chiang Khong rhyolites with the aim to better constrain the age and petrogenesis of the felsic rocks, and to understand their tectonic significance.

Geological background

The Chiang Khong rhyolite is located in the eastern Chiang Rai Province, NW Thailand. According to von Braun and Hahn (1976), the sequences in the study area include mainly Carboniferous–Permian limestone, chert, shale, sandstone and conglomerate, overlain by Triassic conglomerate, sandstone, siltstone, mudstone, with interbedded tuff and shale layers. These sequences are covered in turn by Lower Jurassic reddish brown, purple and pale yellowish green sandstone, siltstone, shale and volcanogenic conglomerate (Fig. 1b; e.g., von Braun and Hahn 1976). The area is characterized by the NNE-trending Doi Yao and Doi Khun Ta Khuan igneous belts, separated by the Cenozoic Chiang Khong basin, which together constitute an important part of the Chiang Khong–Lampang–Tak igneous zone (Fig. 1b; e.g., Barr et al. 2006).

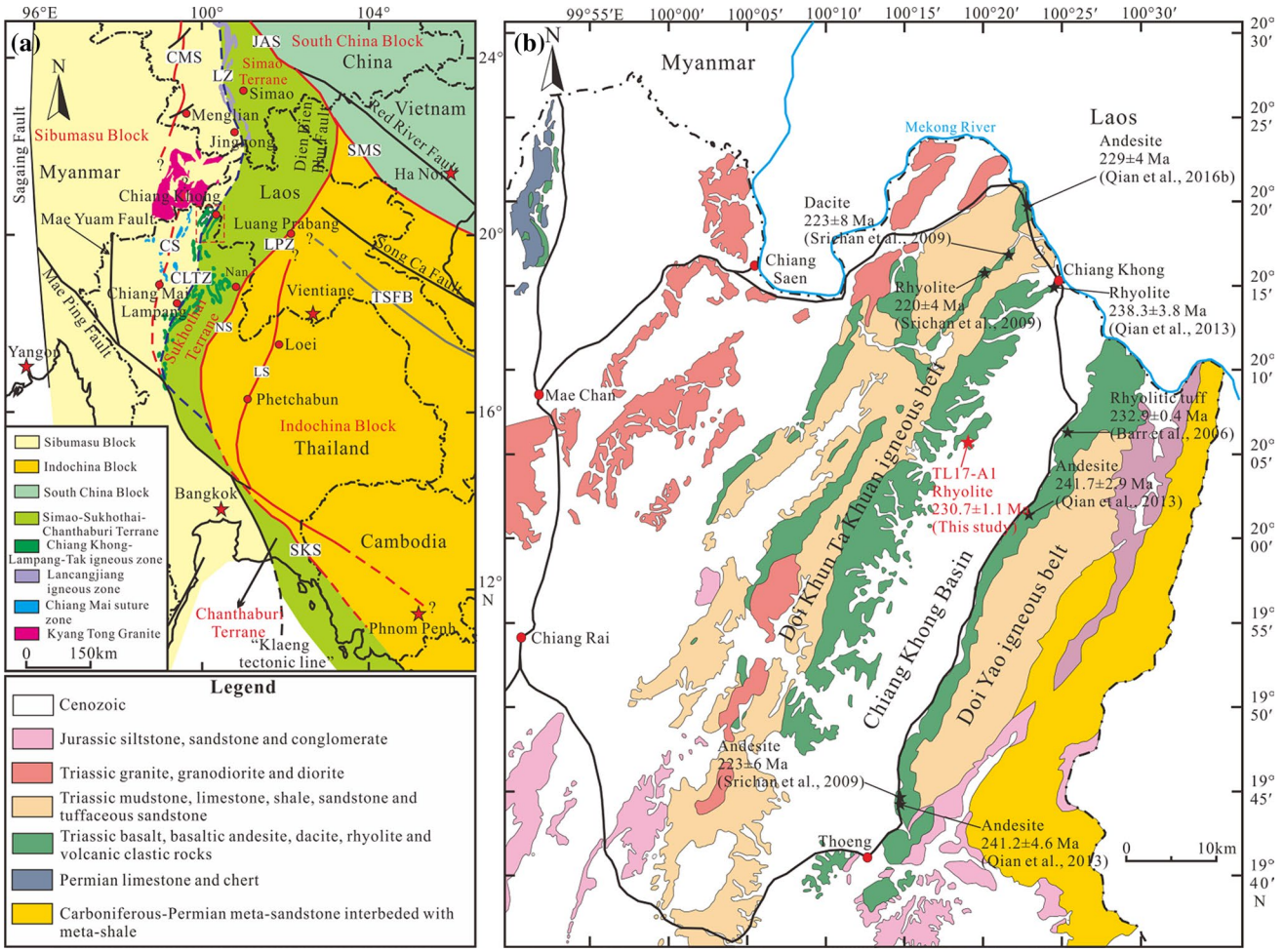

Fig. 1 **a** Tectonic outline of Southeast Asia (Qian et al. 2016a, b), *JAS* Jingshajiang–Ailaoshan suture, *CMS* Changning–Menglian suture, *SMS* Song Ma suture, *CS* Chiang Mai suture, *SKS* Sa Kaeo suture, *NS* Nan suture, *LS* Loei suture, *LPZ* Luang Prabang tectonic zone, *TSFB* Truong Son Fold Belt, *LZ* Lancangjiang igneous zone, *CLTZ* Chiang Khong–Lampang–Tak igneous zone. **b** Simplified geological map of the study area in northern Thailand (revised after von Braun and Hahn 1976; Barr et al. 2006)

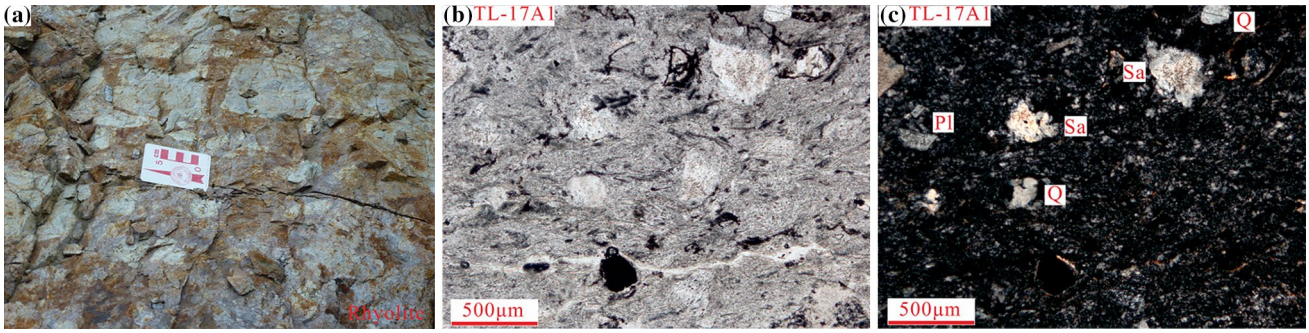

Fig. 2 Field photograph and microscopic photograph for the rhyolite in the Chiang Khong area: **a** rhyolite field photograph and **b**, **c** rhyolitic sample (TL17-A1) with parallel and crossed polarizers, respectively. *Q* quartz, *Sa* sanidine, *Pl* plagioclase

The volcanic sequences are in unconformable contact with the underlying Permian–Triassic sedimentary rocks, and in fault contact with the overlying Late Triassic–Jurassic red beds and Cenozoic sediments. The volcanic rocks are composed of basaltic andesite, andesite, dacite, rhyolite and tuff with volcanoclastic interlayers. The plutonic rocks include granite, granodiorite and diorite of unknown age. The volcanic rocks in the Chiang Khong area have been interpreted as products of two magmatic events that occurred during the Permian–Middle Triassic and the Late Triassic–Jurassic time intervals, largely based on stratigraphic correlations (Jungyusuk and Khositanont 1992). von Braun and Hahn (1976), Phajuy (2001) and Panjasawatwong (2003) suggested that the volcanic rocks in the Doi Khun Ta Khuan and Doi Yao igneous belts formed in a continental arc during the Permian–Triassic period. Barr et al. (2006) reported a zircon age of 232.9 ± 0.4 Ma for the andesite and interpreted that they formed in a continental arc setting. However, Srichan et al. (2009) considered that the Chiang Khong volcanic rocks are Late Triassic (220–223 Ma) products formed in a post-collisional tectonic regime. More recently, Qian et al. (2013) have reported three zircon U–Pb ages of 241.2 ± 4.6, 241.7 ± 2.9 and 238.3 ± 3.8 Ma for andesite and rhyolite samples from the Doi Yao and Doi Khun Ta Khuan igneous belts with geochemical affinities to arc and/or syn-collisional settings. Qian et al. (2016b) also report a zircon age of 229 ± 4 Ma for an andesite sample from an outcrop near the Thailand–Laos border and suggested that the Late Triassic volcanic rocks formed in a post-collisional setting.

The studied rhyolite samples were taken from the Doi Khun Ta Khuan igneous belt west of the Cenozoic Chiang Khong basin in NW Thailand (Fig. 1b). The rhyolites are light red in color and show moderately aphyric to porphyritic textures with subhedral phenocrysts of sanidine, plagioclase and quartz (Fig. 2a, b). Plagioclase phenocrysts show variable degrees of sericitization. The groundmass consists of fine-grained quartz, plagioclase, opaque minerals and glass (Fig. 2c).

Analytical techniques

Zircon grains from a representative rhyolite sample (TL-17A1) were separated by conventional heavy liquid and magnetic techniques. Grains were mounted in epoxy and polished to expose the center of zircon crystals, which were then photographed in transmitted and reflected light. The internal texture of zircons was examined using cathodoluminescence (CL) imaging at the Institute of Geology and Geophysics (IGG), Chinese Academy of Sciences (CAS), Beijing.

Zircons were coated with gold and analyzed using a laser ablation (LA)–ICP–MS at the IGG CAS. The zircon standards CN92-2, 91500 and GJ were used to calibrate the U–Th–Pb ratios. The standard silicate glass NIST 610 was used to optimize the machine. The spot size for data collection was 30 μm. The individual U–Pb analysis is presented with 1σ error, while weighted mean ages are quoted at the 95 % confidence level. The age calculations and plots were made using Isoplot (version 3.0) (Ludwig 2003). Detailed analytical procedure of the LA–ICP–MS technique is similar to those described by Yuan et al. (2004). The analytical data are listed in Table 1.

Zircon Lu–Hf isotopic analysis was carried out using a Geolas-193 laser ablation microprobe, attached to a Neptune multi-collector ICP–MS at the IGG CAS. Zircon Hf isotopic fractionation was corrected using standard zircon 91500. Isobaric interference of ^{176}Yb on ^{176}Hf was corrected by a laboratory-established formula: $\beta_{Yb} = 0.912 \times \beta_{Hf}$. Detailed description of the zircon Hf isotope analytical technique can be found in reference Wu et al. (2006). The zircon U–Pb age was used in the calculation of ε_{Hf} (t) values adopting the chondrule with ^{176}Hf/^{177}Hf = 0.282772 and ^{176}Lu/^{177}Hf = 0.0332 (Blichert and Albarède 1997). Single-stage Hf model

Table 1 LA–ICP–MS zircon U–Pb data of the sample TL-17A1 in the Chiang Khong area, NW Thailand

Analytical spot	Concentration (ppm)				Isotope ratio						Calculated apparent age (Ma)					
	Th	U	Pb	Th/U	$^{207}Pb/^{206}Pb$		$^{207}Pb/^{235}U$		$^{206}Pb/^{238}U$		$^{207}Pb/^{206}Pb$		$^{207}Pb/^{235}U$		$^{206}Pb/^{238}U$	
					Ratio	1σ	Ratio	1σ	Ratio	1σ	Age	1σ	Age	1σ	Age	1σ
TL-17A1-01	87	168	238	0.52	0.051383	0.000956	0.258132	0.005761	0.036437	0.000764	257	44	233	5	231	5
TL-17A1-02	101	177	354	0.57	0.051263	0.000984	0.258867	0.006755	0.036619	0.000880	254	43	234	5	232	5
TL-17A1-03	116	120	443	0.97	0.052306	0.000995	0.265684	0.005912	0.036876	0.000803	298	44	239	5	233	5
TL-17A1-04	75	124	581	0.60	0.051436	0.000977	0.260585	0.005996	0.036738	0.000776	261	43	235	5	233	5
TL-17A1-05	71	110	689	0.65	0.051430	0.000991	0.259480	0.007480	0.036590	0.001020	261	44	234	6	232	6
TL-17A1-06	138	266	987	0.52	0.052477	0.001045	0.265466	0.005935	0.036731	0.000795	306	44	239	5	233	5
TL-17A1-07	62	82	239	0.76	0.051568	0.001071	0.264156	0.006665	0.037105	0.000740	265	53	238	5	235	5
TL-17A1-08	93	97	156	0.96	0.051634	0.000999	0.261383	0.005969	0.036732	0.000805	333	44	236	5	233	5
TL-17A1-09	96	114	456	0.84	0.052183	0.001487	0.255902	0.008210	0.035537	0.000721	295	69	231	7	225	4
TL-17A1-10	131	220	981	0.60	0.051193	0.001406	0.256818	0.008074	0.036420	0.000912	250	69	232	7	231	6
TL-17A1-11	202	171	741	1.18	0.051322	0.000959	0.257300	0.005576	0.036352	0.000729	254	43	232	5	230	5
TL-17A1-12	66	108	410	0.61	0.051337	0.001047	0.258136	0.005808	0.036471	0.000729	257	46	233	5	231	5
TL-17A1-13	56	93	354	0.60	0.051531	0.000908	0.258474	0.006044	0.036346	0.000784	265	36	233	5	230	5
TL-17A1-14	160	168	1023	0.95	0.051597	0.000928	0.259527	0.005761	0.036461	0.000745	333	38	234	5	231	5
TL-17A1-15	82	114	652	0.72	0.051545	0.000986	0.261735	0.005969	0.036839	0.000778	265	44	236	5	233	5
TL-17A1-16	73	95	375	0.77	0.051180	0.000968	0.259080	0.005770	0.036220	0.000640	249	43	234	5	229	4
TL-17A1-17	98	101	603	0.97	0.053190	0.001196	0.263670	0.007250	0.036240	0.000780	337	54	238	6	230	5
TL-17A1-18	79	126	867	0.63	0.051371	0.000985	0.255847	0.006393	0.036101	0.000800	257	44	231	5	229	5
TL-17A1-19	88	139	1014	0.63	0.051640	0.001223	0.256440	0.007960	0.036000	0.001100	270	54	232	6	228	7
TL-17A1-20	103	151	1004	0.68	0.052070	0.001171	0.260650	0.005660	0.036150	0.000580	289	50	235	5	229	4

ages were calculated relative to the depleted mantle with $^{176}Hf/^{177}Hf = 0.28325$ and $^{176}Lu/^{177}Hf = 0.0384$ (Griffin et al. 2000), and two-stage Hf model ages were calculated with a mean $^{176}Lu/^{177}Hf = 0.015$ of the average continental crust (Amelin et al. 1999). Zircon oxygen isotopic analysis was measured using the CAMECA 1280 at IGG CAS. The Cs^+ ion beam was accelerated to 10 kV, with an intensity of ~2 nA. The analysis site was the same as for U–Pb dating, and the spot size about 20 μm in diameter. The normal incidence electron flood gun was used to compensate for sample charging. The nuclear magnetic resonance (NMR) was used for stabilizing magnetic field. Oxygen isotopes were measured in multi-collector mode with two off-axis Faraday cups. Analytical procedures are similar to that described by Li et al. (2010a). The instrumental mass fractionation factor (IMF) was corrected using Penglai zircon standard with $\delta^{18}O$ value of 5.31 ‰ (Li et al. 2010b). The internal precision of a single analysis was generally better than 0.20 ‰ (1σstandard error) for $^{18}O/^{16}O$ ratio. The external precision measured by the reproducibility of repeated analyses of Penglai standard is 0.27 ‰ ($n = 8$). During the course of this study, an in-house zircon standard Qinghu was also measured as an unknown together with other unknowns. Four measurements of Qinghu zircon yield a weighted mean of $\delta^{18}O = 5.54 \pm 0.32$ ‰, which is consistent within errors with the reported value of 5.4 ± 0.2 ‰ (Li et al. 2013). Zircon Lu–Hf and oxygen isotopic analyzed data are listed in Table 2.

Samples were selected for whole-rock elemental and Sr–Nd isotopic analyses, and were crushed to 200-mesh using an agate mill. The major oxides were analyzed by wavelength X-ray fluorescence spectrometry at the State Key Laboratory of Isotope Geochemistry, Guangzhou Institute of Geochemistry (GIG), Chinese Academy of Sciences (CAS). Trace element analyses were performed at the same laboratory using a Perkin-Elmer Sciex ELAN 6000 ICP–MS. Detailed sample preparation and analytical procedure followed Li et al. (2002). Sr–Nd isotopic ratios were measured on the Micromass IsoProbe™ MC–ICPMS at the GIG. The analytical procedures are the same as reported by Wei et al. (2002).The total procedure blanks were in the range of 200–500 pg for Sr and ≤50 pg for Nd. The mass fractionation corrections for Sr and Nd isotopic ratios are based on $^{86}Sr/^{88}Sr = 0.1194$ and $^{146}Nd/^{144}Nd = 0.7219$, respectively. The measured $^{87}Sr/^{86}Sr$ ratios of the (NIST) SRM987 standard are 0.710265 ± 12 (2σ), and the measured $^{143}Nd/^{144}Nd$ ratios of the La Jolla standard are 0.511862 ± 10 (2σ). The whole-rock elemental and two Sr and Nd isotopic data of the selected samples are given in Table 3.

Table 2 Zircon in situ Hf and O isotopic compositions of sample TL-17A1

Analytical spot	T (Ma)	$^{176}Hf/^{177}Hf$	1σ	$^{176}Yb/^{177}Hf$	$^{176}Lu/^{177}Hf$	$\varepsilon_{Hf}(t)$	T_{DM1} (Ga)	T_{DM2} (Ga)	$\delta^{18}O$	2σ
TL-17A1-01	231	0.282800	0.000015	0.055611	0.001491	5.8	0.65	0.75	5.7	0.35
TL-17A1-02	232	0.282825	0.000018	0.105760	0.002631	6.6	0.63	0.71	5.6	0.22
TL-17A1-03	233	0.282772	0.000021	0.116577	0.002975	4.7	0.72	0.81	5.6	0.28
TL-17A1-04	233	0.282795	0.000020	0.072046	0.001899	5.6	0.66	0.76	5.9	0.33
TL-17A1-05	232	0.282823	0.000015	0.068604	0.001751	6.6	0.62	0.71	5.4	0.32
TL-17A1-06	233	0.282785	0.000019	0.067170	0.001672	5.3	0.67	0.78	5.9	0.20
TL-17A1-07	235	0.282831	0.000021	0.109840	0.002732	6.8	0.63	0.70	5.7	0.18
TL-17A1-08	233	0.282806	0.000020	0.142681	0.003716	5.7	0.68	0.75	5.3	0.46
TL-17A1-09	225	0.282782	0.000019	0.100739	0.002599	4.9	0.70	0.79	5.4	0.30
TL-17A1-10	231	0.282769	0.000022	0.054670	0.001420	4.7	0.69	0.80	5.7	0.20
TL-17A1-11	230	0.282871	0.000020	0.142844	0.003465	8.0	0.58	0.64	5.8	0.29
TL-17A1-12	231	0.282872	0.000019	0.118613	0.002924	8.2	0.57	0.63	5.3	0.23
TL-17A1-13	230	0.282840	0.000021	0.114545	0.002875	7.0	0.62	0.69	5.9	0.29
TL-17A1-14	231	0.282892	0.000019	0.106555	0.002553	8.9	0.53	0.59	5.4	0.25
TL-17A1-15	233	0.282916	0.000020	0.150517	0.003461	9.7	0.51	0.56	5.5	0.37
TL-17A1-16	229	0.282880	0.000024	0.165600	0.003766	8.3	0.57	0.62		
TL-17A1-17	230	0.282982	0.000020	0.150402	0.003386	12.0	0.41	0.44		
TL-17A1-18	229	0.282873	0.000019	0.133701	0.003023	8.1	0.57	0.63		
TL-17A1-19	228	0.282824	0.000023	0.115491	0.002611	6.5	0.63	0.71		
TL-17A1-20	229	0.282808	0.000021	0.120476	0.002789	5.9	0.66	0.74		

$\varepsilon_{Hf}(t) = [^{176}Hf/^{177}Hf_Z/^{176}Hf/^{177}Hf_{CHUR(t)}-1] \times 10{,}000$

$^{176}Hf/^{177}Hf_{CHUR(t)} = {}^{176}Hf/^{177}Hf_{CHUR(0)}-{}^{176}Lu/^{177}Hf_{CHUR} \times (e^{\lambda t}-1)$

$T_{DM1} = (1/\lambda) \times \ln[1 + (^{176}Hf/^{177}Hf_{DM}-{}^{176}Hf/^{177}Hf_Z)/(^{176}Lu/^{177}Hf_{DM}-{}^{176}Lu/^{177}Hf_Z)]$

$T_{DM2} = T_{DM1}-(T_{DM1}-T) \times [(f_C-f_Z)/(f_C-f_{DM})]$

$f_{Lu/Hf} = {}^{176}Hf/^{177}Hf/^{176}Lu/^{177}Hf_{CHUR}-1$

Where f_C, f_Z and f_{DM} are the $f_{Lu/Hf}$ values of the continental crust, zircon sample and the depleted mantle

Subscript Z = analyzed zircon sample, CHUR = chondritic uniform reservoir, DM = depleted mantle. T = zircon U–Pb age

$\lambda = 1.867 \times 10^{-11}$ year^{-1}, decay constant of ^{176}Lu (Söderlund et al. 2004)

$^{176}Hf/^{177}Hf_{DM} = 0.28325$, $^{176}Lu/^{177}Hf_{DM} = 0.0384$ (Griffin et al. 2000)

Present-day $^{176}Hf/^{177}Hf_{CHUR(0)} = 0.282772$; $^{176}Lu/^{177}Hf_{CHUR} = 0.0332$ (Blichert and Albarède 1997)

$(^{176}Lu/^{177}Hf)_{CC} = 0.015$, $(^{176}Hf/^{177}Hf)_{CC} = 0.28325$ (Amelin et al. 1999)

Analytical results

Zircon U–Pb dating

The majority of zircon grains from the rhyolite sample TL-17A1 are transparent, euhedral and light brown, and exhibit oscillatory zoning in CL images (Wu and Zheng 2004) (Fig. 3). Twenty analytical spots on 20 zircon grains have Th and U concentrations ranging from 56 to 160 ppm and 82 to 266 ppm, respectively, with Th/U ratios in the range of 0.52–1.18. All analyses yield a weighted mean $^{206}Pb/^{238}U$ age of 230.7 ± 1.1 Ma with MSWD = 0.98 (Fig. 3), interpreted as the crystallization age of the rhyolite.

Zircon Hf and O isotopic compositions

In situ Hf and oxygen isotopic compositions were analyzed on the dated zircons from sample TL-17A1 (Table 2). The $^{176}Lu/^{177}Hf$ ratios of 20 zircon grains range from 0.001420 to 0.003766, indicating that only a small amount of radiogenic Hf has accumulated since the zircons crystallized (Griffin et al. 2000). These grains have positive $\varepsilon_{Hf}(t)$ values ranging from 4.7 to 12.0, with corresponding T_{DM1} and T_{DM2} in the range of 0.41–0.72 and 0.44–0.81 Ga, respectively (Fig. 4a). The measured zircon grains have a restricted range of oxygen isotopic compositions. Fifteen zircon grains yield mantle-like $\delta^{18}O$ values of 5.3–5.9 ‰ (Table 2; Fig. 4b). The whole-rock $\delta^{18}O$ in

Table 3 Major oxides, trace element analytical data and Sr–Nd isotopic compositions of the rhyolites in the Chiang Khong area, NW Thailand

Sample	TL17-A1	TL17-A2	TL17-A3	TL17-A4	TL17-A5	TL17-A6	TL17-A7
SiO_2	73.68	76.62	76.99	71.33	73.98	70.57	70.88
TiO_2	0.43	0.31	0.30	0.62	0.51	0.40	0.29
Al_2O_3	13.87	13.01	12.97	14.36	13.06	15.88	14.38
Fe_2O_3t	2.54	1.43	1.86	3.75	3.04	2.31	3.35
MnO	0.02	0.01	0.02	0.03	0.05	0.06	0.04
MgO	0.13	0.08	0.04	0.27	0.14	0.81	0.41
CaO	0.41	0.15	0.32	0.56	0.97	1.51	0.57
Na_2O	7.02	6.22	6.42	6.65	6.58	1.73	4.15
K_2O	1.65	2.07	1.15	1.85	1.12	4.83	5.21
P_2O_5	0.09	0.001	0.03	0.16	0.12	0.04	0.04
LOI	0.55	0.48	0.29	0.69	0.73	1.90	0.78
Total	100.40	100.38	100.39	100.27	100.31	100.05	100.11
A/CNK	0.99	1.02	1.05	1.03	0.95	1.47	1.06
A/NK	1.04	1.04	1.10	1.11	1.09	1.97	1.15
Sc	18.3	14.4	17.9	23.4	22.1	12.3	21.9
V	9	8	5	31	13	10	10
Cr	3.0	2.8	3.3	8.2	3.9	3.9	11.2
Co	1.3	0.6	0.4	3.3	2.2	1.7	2.2
Ni	0.4	1.5	0.4	2.3	0.5	1.4	4.9
Rb	30.4	40.5	18.1	51.0	24.7	184.0	190.7
Sr	87	54	61	147	116	163	86
Y	22.71	10.20	16.87	25.32	28.05	44.38	34.20
Zr	185.5	239.3	223.3	205.6	189.8	280.0	316.8
Nb	9.06	11.77	11.24	9.71	9.27	16.37	25.11
Ba	285	288	157	404	208	922	848
La	12.07	5.83	23.73	19.14	28.49	64.39	33.98
Ce	31.38	11.33	55.10	40.01	53.97	118.11	79.02
Pr	4.21	1.76	5.45	5.33	6.50	13.43	10.10
Nd	17.13	6.76	19.65	20.13	24.79	49.96	38.58
Sm	3.91	1.56	3.57	4.32	5.20	8.74	7.92
Eu	0.80	0.35	0.81	1.01	1.23	1.98	1.68
Gd	3.60	1.38	3.35	4.16	4.75	8.48	6.61
Tb	0.69	0.29	0.57	0.73	0.83	1.38	1.21
Dy	4.03	1.79	3.35	4.50	4.74	7.77	6.93
Ho	0.91	0.45	0.73	1.01	1.07	1.74	1.52
Er	2.69	1.37	1.97	2.93	3.11	4.82	4.14
Tm	0.41	0.22	0.31	0.46	0.46	0.75	0.62
Yb	2.60	1.50	1.99	3.05	3.00	4.87	4.16
Lu	0.38	0.22	0.29	0.46	0.44	0.77	0.61
Hf	5.01	6.45	6.21	5.28	5.04	7.92	7.81
Ta	0.64	0.81	0.78	0.69	0.65	1.07	1.56
Pb	7.06	6.71	5.92	12.70	7.80	26.62	7.11
Th	8.23	8.60	9.32	9.02	8.74	14.40	16.97
Eu/Eu*	0.64	0.71	0.70	0.72	0.74	0.69	0.69
$(La/Yb)_N$	3.33	2.78	8.56	4.50	6.82	9.48	5.86
$(Gd/Yb)_N$	1.14	0.76	1.39	1.13	1.31	1.44	1.31
$^{87}Rb/^{86}Sr$	1.016			1.002			
$^{147}Sm/^{144}Nd$	0.138			0.130			
$^{87}Sr/^{86}Sr$	0.708304			0.708565			
2σ	0.000007			0.000006			

Table 3 continued

Sample	TL17-A1	TL17-A2	TL17-A3	TL17-A4	TL17-A5	TL17-A6	TL17-A7
$^{143}Nd/^{144}Nd$	0.512618			0.512595			
2σ	0.000004			0.000004			
$(^{87}Sr/^{86}Sr)_i$	0.70497			0.70527			
ε_{Nd} (*t*)	1.33			1.13			
T_{DM2} (Ga)	0.80			0.81			

Fe_2O_3t represents total Fe oxides, $Eu/Eu^* = 2 \times Eu_N/(Sm_N + Gd_N)$, $^{147}Sm/^{144}Nd = 0.1967$, $^{143}Nd/^{144}Nd = 0.512638$, which are used for the calculation. ε_{Nd} (*t*) is calculated by assuming 231 Ma

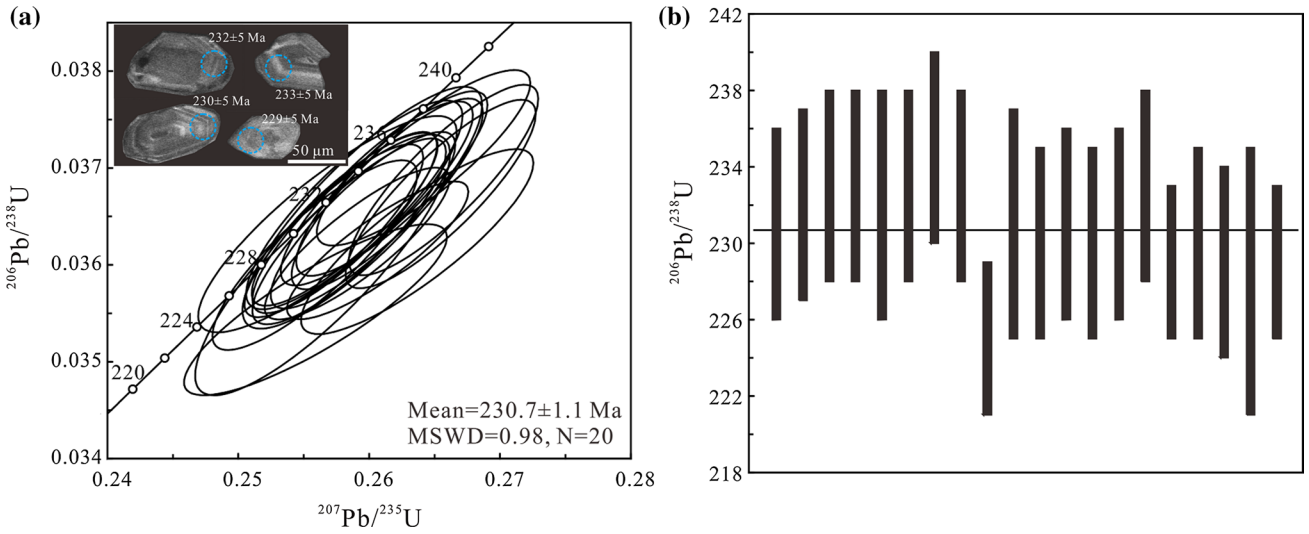

Fig. 3 **a** LA–ICP–MS zircon U–Pb concordia diagram and **b** weighted average diagram for rhyolite sample (TL17-A1) in the Chiang Khong area with cathodoluminescence (CL) image of representative zircon grains

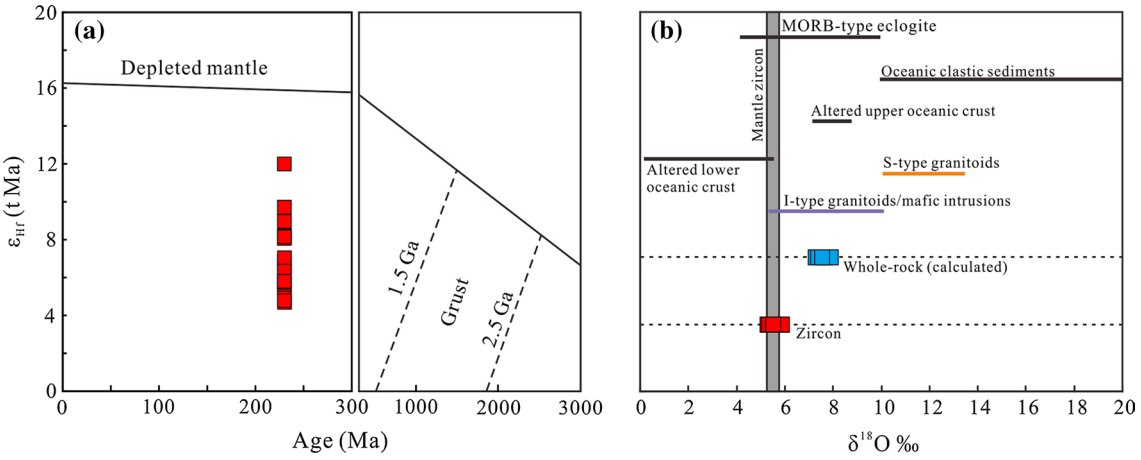

Fig. 4 Plots of **a** age (Ma) versus ε_{Hf} (*t*) and **b** oxygen isotopic compositions for zircon grains from sample TL17-A1. Also shown for MORB (Eiler et al. 2000), altered upper and lower oceanic crust (Gregory and Taylor 1981; Cocker et al. 1982), mafic rocks and I-, and S-type granitoids (Eiler et al. 2000). Whole-rock $\delta^{18}O$ is calculated using whole-rock $\delta^{18}O$ = zircon $\delta^{18}O + 0.0612 \times (wt\% SiO_2) - 2.5$ (Valley et al. 2005)

equilibrium with zircon $\delta^{18}O$ can be approximated by the empirical linear relationship: whole-rock $\delta^{18}O \approx$ zircon $\delta^{18}O + 0.0612 \times (wt\% SiO_2) - 2.5$ (Valley et al. 2005). The zircon grains used to constrain the crystallization age yield calculated whole-rock $\delta^{18}O$ of 7.4–7.9 ‰ (Fig. 4b).

Whole-rock geochemistry

Contents of major oxides are normalized to 100 % on a volatile-free basis. The seven rhyolite samples in this study display a moderate range of SiO_2 (71.36–76.92 wt%), low TiO_2 (0.29–0.62 wt%), low MgO (0.04–0.82 wt%) and high Al_2O_3 (12.95–16.18 wt%) (Table 3; Fig. 4). In the TAS diagram (Fig. 5a) (after Le Bas et al. 1986), these samples fall in the field of subalkalic rhyolite and that of the post-collisional granitoids (Luo and Yin 1988; Jian et al. 2003; Zhu et al. 2011), similar to those reported by Barr et al. (2006), Srichan et al. (2009) and Qian et al. (2013). Most of the samples straddle the metaluminous–peraluminous boundary with A/CNK [molar $Al_2O_3/(CaO + Na_2O + K_2O)$] values of 0.95–1.06 with all except the outlier (sample TL-17 A6 at 1.47) plotting as I-type granite (Fig. 5b). The differentiation index (DI) (DI = Q+Or + Ab + Ne + Lc + Kp) varies between 82 and 97, suggesting that the magma was highly evolved. In the A.R.–SiO_2 diagram (Fig. 5c) (after Wright 1969), most samples plot in the alkaline field. In addition, the 10000 × Ga/Al ratios of the rhyolites range from 1.05 to 1.94 and most samples plot within the field of I- and S-type granite (Whalen et al. 1987) (Fig. 6). All these features suggest that these samples can be classified as highly fractionated I-type rhyolites. All samples exhibit REE fractionation with $(La/Yb)_N$ (N herein refers to chondrite-normalized value) of 2.78–9.48, $(Gd/Yb)_N$ of 0.76–1.44 and Eu/Eu* of 0.64–0.74 (Table 3; Fig. 7a). As shown in the primitive mantle-normalized multi-element spidergram (Sun and McDonough 1989) (Fig. 7b), these samples are characterized by enrichment in large ion lithophile elements (LILEs) and depletion in high field strength elements (HFSEs) (e.g., Nb, Ta and Ti) with Th/La = 0.22–1.47 and Nb/La = 0.25–2.02. Most samples are broadly similar to the Chiang Khong Triassic rhyolites samples (Barr et al. 2006; Srichan et al. 2009; Qian et al. 2013). One outlier sample (TL17-A2) with lower Y and REE is also similar to the Chiang Khong Triassic rhyolite sample reported by Barr et al. (2006). In comparison with the high-Mg post-collisional volcanic rocks in the Lancangjiang igneous zone, the Chiang Khong Triassic rhyolites samples (e.g., Barr et al. 2006; Srichan et al. 2009; Qian et al. 2013) do not show negative Th anomalies, but have negative Sr anomalies, are similar to the high-Al post-collisional volcanic rocks in the Lancangjiang igneous zone (Fig. 7b) (e.g., Wang et al. 2010).

The Sr–Nd isotopic analytical results for two selected samples are presented in Table 3. The initial Sr–Nd isotopic ratios were calculated using the age of 231 Ma. The two samples have $^{87}Sr/^{86}Sr$ (i) ratios of 0.70497 and 0.70527. The ε_{Nd} (t) values fall at +1.1 and +1.3, corresponding to Neoproterozoic Nd model ages (Table 3; Fig. 8). The two ε_{Nd} (t) values are slightly higher than those of the high-Al post-collisional volcanic rocks in the Lancangjiang and Chiang Khong–Lampang–Tak igneous zones (Wang et al. 2010; Qian et al. 2016b), but lower than the high-Mg post-collisional volcanic rocks in the Lancangjiang igneous zone (Fig. 8) (Wang et al. 2010).

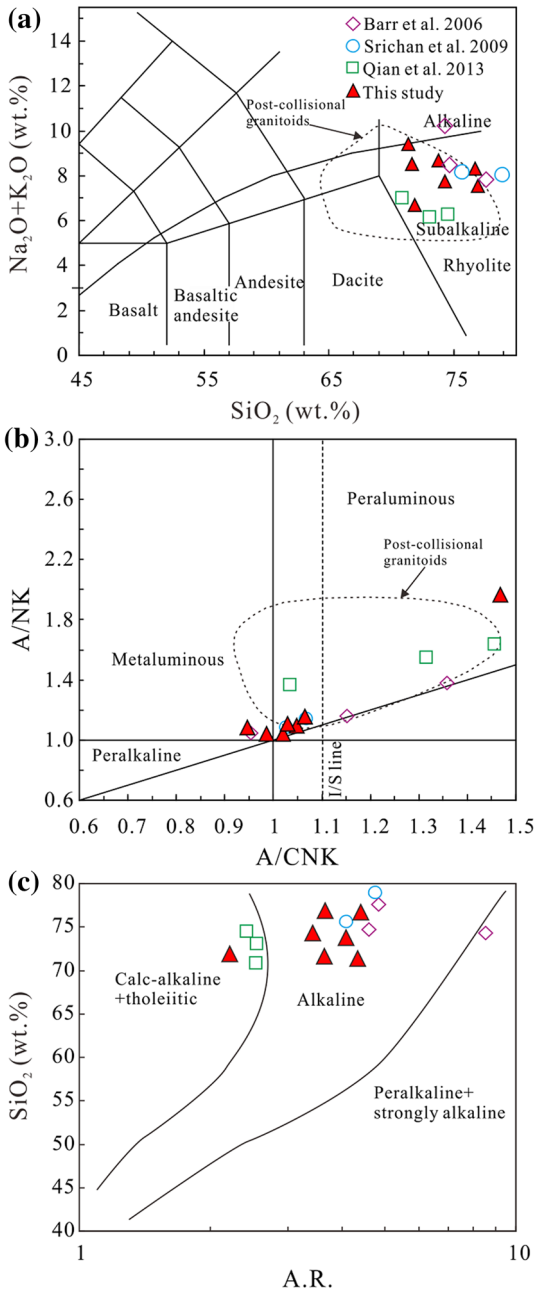

Fig. 5 **a** SiO_2 versus $Na_2O + K_2O$ (TAS) (after Le Bas et al. 1986), **b** A/CNK versus A/NK and **c** A.R. versus SiO_2 (after Wright 1969) classification diagrams for the Late Triassic rhyolites in the Chiang Khong area, NW Thailand. A.R.: (alkalinity ratio) = $[Al_2O_3 + CaO + (Na_2O + K_2O)]/[Al_2O_3 + CaO - (Na_2O - K_2O)]$ (wt%). The field of the post-collisional granitoids is from Luo and Yin (1988), Jian et al. (2003) and Zhu et al. (2011). The data of Triassic rhyolites are from Barr et al. (2006), Srichan et al. (2009) and Qian et al. (2013)

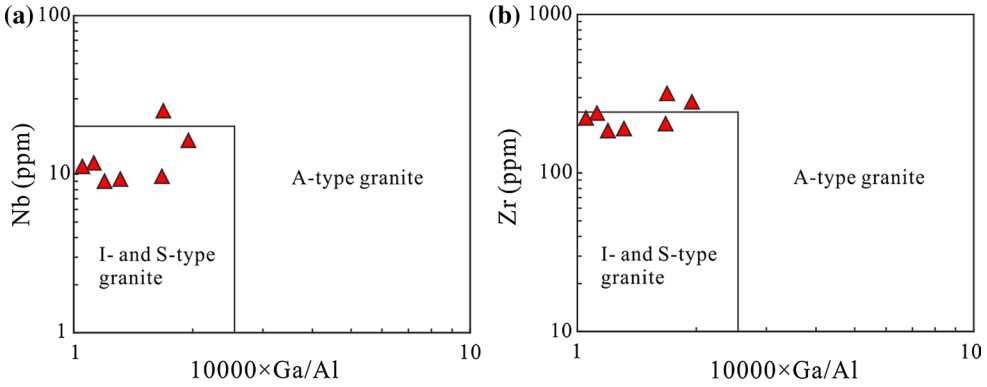

Fig. 6 **a** 10,000 × Ga/Al versus Nb and **b** 10,000 × Ga/Al versus Zr diagrams (after Whalen et al. 1987) for the Late Triassic rhyolites in the Chiang Khong area, NW Thailand

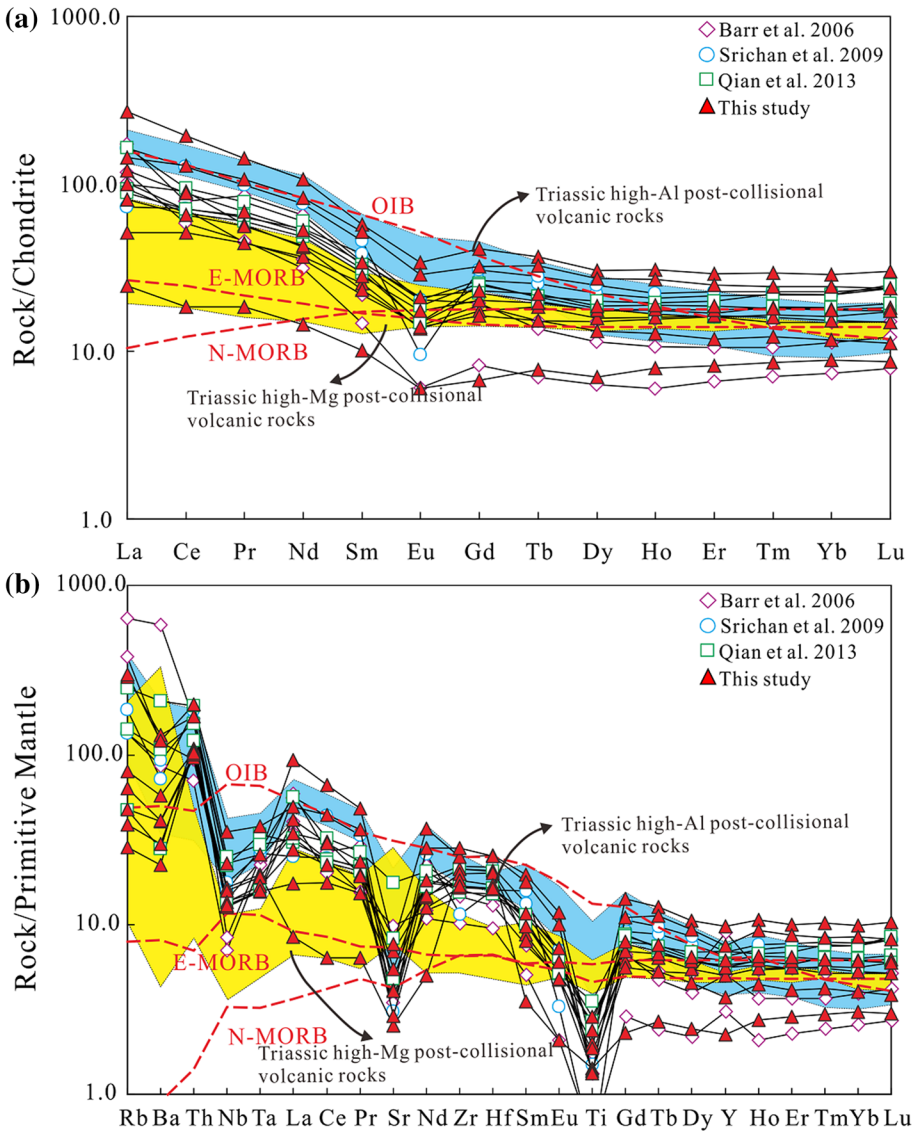

Fig. 7 **a** Chondrite-normalized REE patterns and **b** Primitive mantle–normalized trace element spidergrams for the Late Triassic rhyolites in the Chiang Khong area, NW Thailand. Also shown are the patterns of N-MORB, E-MORB and OIB. Normalized values for chondrite and primitive mantle are from Sun and McDonough (1989). The data of the Lancangjiang Late Triassic high-Al and high-Mg post-collisional volcanic rocks are from Wang et al. (2010). The data of Late Triassic rhyolites from the Chiang Khong area are from Barr et al. (2006), Srichan et al. (2009) and Qian et al. (2013), respectively

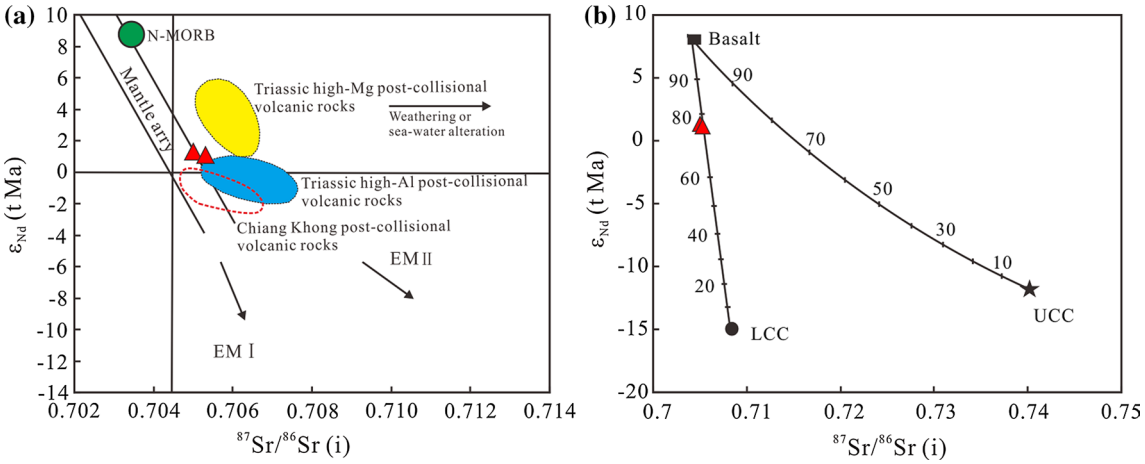

Fig. 8 **a** $^{87}Sr/^{86}Sr$ (*i*) versus ε_{Nd} (*t*) and **b** the mixing model for the Late Triassic rhyolites in the Chiang Khong area, NW Thailand. The fields of Lancangjiang post-collisional volcanic rocks and Chiang Khong post-collisional volcanic rocks are from Wang et al. (2010) and Qian et al. (2016b), respectively. The fields of EMI and EMII are from Zindler and Hart (1986). The mixing model of two end members: (Atherton and Petford 1993) basalt representing the mantle-derived components ($^{87}Sr/^{86}Sr = 0.704$, $\varepsilon_{Nd} = +8$), (Audétat 2010) crustal components (*LCC* lower continental crust, $^{87}Sr/^{86}Sr = 0.708$, $\varepsilon_{Nd} = -15$; *UCC* upper continental crust, $^{87}Sr/^{86}Sr = 0.740$, $\varepsilon_{Nd} = -12$), the end member data from Wu et al. (2003b)

Discussion

Petrogenesis

The studied samples are relatively fresh, and all samples show low loss on ignition (LOI) contents (0.29–1.90 wt%), suggesting that post-eruption alteration or weathering is not severe. Furthermore, the homogenous mantle-like $\delta^{18}O$ values, positive ε_{Hf} (*t*) values (Fig. 4a, b), and two representative Sr–Nd isotopic compositions (Fig. 8) suggest that the crustal contamination did not play a significant role during magma evolution.

As described earlier, our samples can be classified as highly fractionated I-type rhyolites. Three processes have been proposed for the origin of I-type rhyolites: (1) mixing between crust-derived felsic and mantle-derived mafic magmas (e.g., Wu et al. 2003b; Clemens et al. 2011), (2) fractional crystallization of mantle-derived basaltic parental magma (e.g., Barth et al. 1995; Rapp and Watson 1995; Wu et al. 2003b) and (3) partial melting of the mafic to intermediate crust, followed by extensive fractional crystallization (e.g., Wu et al. 2003b; Zhao and Zhou 2009; Liu et al. 2014; Zhang et al. 2015). Below we assess each of these scenarios and their applicability to the Chiang Khong rhyolites.

The magma mixing model involving the mingling of isotopically primitive mantle-derived material with a partial melt of relatively evolved crust would produce a wide range of isotopic and geochemical signatures (Zhang et al. 2015). However, zircon grains from our Chiang Khong rhyolite samples have homologous mantle-like $\delta^{18}O$ values of 5.3–5.9 ‰. They also show mantle-like $^{87}Sr/^{86}Sr$ (*i*) ratios and ε_{Nd} values. Accordingly, the magma mixing model proposed is not feasible for the Chiang Khong rhyolites.

In general, large volumes of basaltic magma are needed to produce small amounts of silicic rock (Peccerillo et al. 2003). Experiments also have shown that mafic magmas can produce 12–25 wt% of felsic magmas by differentiation (Sisson et al. 2005). Late Triassic volcanic rocks are relatively common in the Chiang Khong area (Srichan et al. 2009; Barr and Charusiri 2011; Qian et al. 2016b), however, mafic and intermediate rocks are not widely distributed and where present their ε_{Nd} values of −1.92 to −0.32 (Qian et al. 2016b) are lower than the Chiang Khong rhyolites. Therefore, fractional crystallization of mantle-derived basaltic magma is unlikely for the Chiang Khong rhyolites.

Partial melting of the mafic to intermediate crust is the most likely explanation for the formation of the Chiang Khong rhyolites. Trace element modeling (Fig. 9) indicates that extensive fractional crystallization took place after the initial magma formation with biotite, plagioclase, hornblende and allanite being important fractionating phases. Two selected samples have low $^{87}Sr/^{86}Sr$ (*i*) ratios and positive ε_{Nd} (*t*) values (Fig. 8a), and the modeling based on isotopic data (Fig. 8b) shows that no upper crustal component has been added to the magma source. Zircon Hf and O isotopic compositions are typical of mantle values. All these isotopic characteristics suggest that mantle-derived materials were involved in the source region of the Chiang Khong rhyolites. Their Neoproterozoic Nd model ages (0.80–0.81 Ga) and Hf T_{DM1} (0.41–0.72 Ga) are much older than the eruption age of 231 Ma. Moreover, these samples have

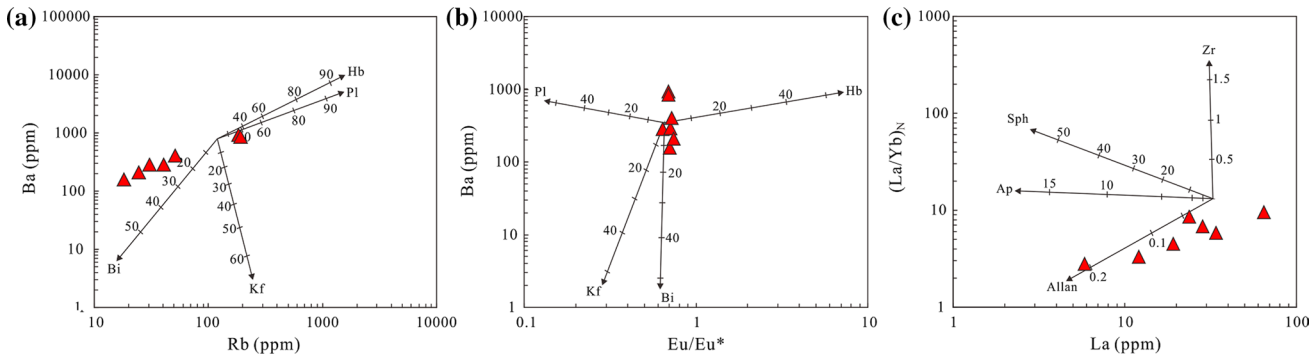

Fig. 9 **a** Rb versus Ba, **b** Eu/Eu* versus Ba and **c** La versus $(La/Yb)_N$ diagrams (after Wu et al. 2003a; Zhang et al. 2015) for the Late Triassic rhyolites in the Chiang Khong area, NW Thailand

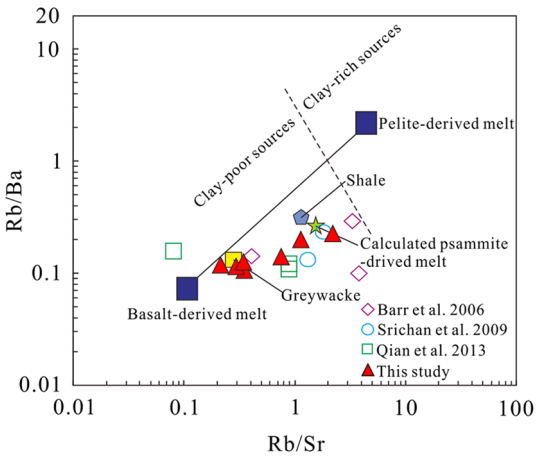

Fig. 10 Rb/Sr versus Rb/Ba diagram (after Sylvester 1998) for the Late Triassic rhyolites in the Chiang Khong area, NW Thailand

low Rb/Sr and Rb/Ba ratios and plot within the clay-poor field (Fig. 10), indicating little or no clay-rich sedimentary contribution to the magma. Therefore, the geochemistry and isotopic compositions of Chiang Khong rhyolites argue for a derivation from partial melting of juvenile mafic lower crust and en route to the surface the melts experienced extensive fractional crystallization, with removal of biotite, hornblende, plagioclase and allanite.

Tectonic implications

Triassic felsic rocks are widely distributed along the Chiang Khong–Lampang–Tak igneous zone in NW Thailand. The rhyolite exposed in the Lampang area of the central igneous zone was dated at ca. 240 Ma (Barr et al. 2000). The Chiang Khong rhyolite in the northern part of the igneous zone gave zircon ages of 220–238 Ma (Barr et al. 2006; Srichan et al. 2009 ; Qian et al. 2013). Similar ages of 220–242 Ma have been obtained from the mafic–intermediate volcanic rocks in the northern part of the igneous zone (Srichan et al. 2009; Qian et al. 2013, 2016b). Recent studies have suggested that the Chiang Khong–Lampang–Tak igneous zone can be linked with the Lancangjiang igneous zone to the north based on geochronological and geochemical data of volcanic rocks (Barr et al. 2000, 2006; Barr and Charusiri 2011; Qian et al. 2013, 2016b). Within the Lancangjiang igneous zone, abundant Middle–Late Triassic igneous rocks have been identified and are generally interpreted to have formed in collision-related settings (Peng et al. 2006, 2013; Wang et al. 2010; Kong et al. 2012; Wang et al. 2012; Dong et al. 2013). Meanwhile, granitic rocks from the Kyaing Tong Granite between the Chiang Khong–Lampang–Tak and Lancangjiang igneous zones (Fig. 1a) were dated at 219–220 Ma by Gardiner et al. (2015) who suggest that the closure and suturing of the Paleo-Tethys occurred at ca. 230 Ma in northern Thailand and eastern Myanmar. Our zircon age of 231 Ma from the Chiang Khong rhyolite is consistent with the published geochronological data, and taken together, these suggest a Middle–Late Triassic collisional orogenesis along the Chiang Khong–Lampang–Tak and Lancangjiang igneous zones, and the Kyaing Tong Granite in eastern Myanmar.

The studied Chiang Khong rhyolites belong to the high fractionated I-type rhyolites. I-type igneous rocks are most abundant in Andean-type continental arc settings or post-collisional settings (Roberts and Clemens 1993). Available data have established that the collision between the Indochina and Sibumasu blocks occurred during the Middle–early Late Triassic (Srichan et al. 2009; Wang et al. 2010; Qian et al. 2013; Fan et al. 2015; Qian et al. 2016b). In addition, the studied rhyolites are in fault contact with Late Triassic–Jurassic red beds and Cenozoic sediments (von Braun and Hahn 1976; Jungyusuk and Khositanont 1992; Srichan et al. 2009). This stratigraphic relationship supports the Late Triassic as the time of collision. Therefore, the genesis of the Late Triassic Chiang Khong rhyolites was likely associated with a collisional setting. Moreover,

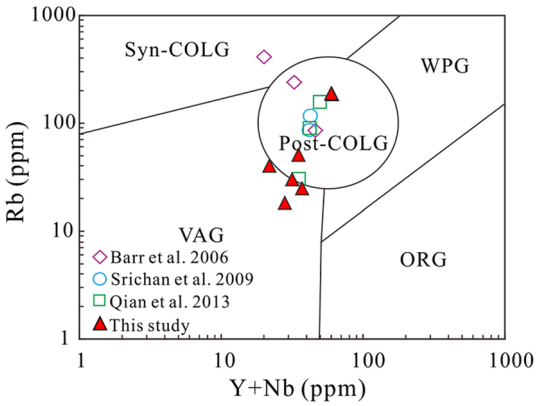

Fig. 11 Y + Nb versus Rb (after Pearce 1996) discrimination diagram for the Late Triassic rhyolites in the Chiang Khong area, NW Thailand. The other data of Late Triassic rhyolites from the Chiang Khong area are from Barr et al. (2006), Srichan et al. (2009) and Qian et al. (2013), respectively. *WPG* within-plate granite, *VAG* volcanic arc granite, *Syn-COLG* syn-collisional granite, *post-COLG* post-collision granite, *ORG* ocean ridge granite

in the Y + Nb − Rb (after Pearce 1996) discrimination diagram (Fig. 11), most rhyolite samples from the Chiang Khong area fall in the fields of post-collisional and volcanic arc granites. This is consistent with the conclusions of recent studies by Srichan et al. (2009) and Qian et al. (2016b) on other Late Triassic volcanic rocks in the Chiang Khong–Lampang–Tak igneous zone. From the geochemistry in combination with the geochronology data, we propose that the rhyolites in the Chiang Khong area are equivalent with the post-collisional volcanic rocks of the Xiaodingxi and Manghuihe formations in the Lancangjiang igneous zone (Wang et al. 2010; Peng et al. 2013).

Our Chiang Khong rhyolite samples are characterized by relatively high ε_{Hf} (t) and ε_{Nd} (t) values and have mantle-like O isotopic compositions and probably originated from partial melting of juvenile mafic lower crust. Srichan et al. (2009) suggested that the Late Triassic volcanic rocks in the Chiang Khong area may be related to gravitational collapse of the thickened crust according to the geochemical similarity between the rift-related Whitsunday volcanic province and the Chiang Khong suites. However, the gravitational collapse is a slow passive process and usually occurs in the continental lower crust and does not cause the extensive magma activity (Zhang et al. 2006). Therefore, these rhyolite samples in the Chiang Khong area may be related to another mechanism. It is well known that continuous subduction can result in the HP–UHP metamorphism of the subducting slab to form eclogite, and ultimately lead to detachment/break-off of the eclogitized slab (e.g., Bird 1979; Cooke and O'Brien 2001). Following the slab detachment, the upwelling asthenospheric mantle not only heats to melt the lithosphere and cause partial melting of the crust and mantle wedge, but also supplies asthenospheric materialto generate the high ε_{Hf} (t) and ε_{Nd} (t) magma (Davies and von Blanckenburg 1995; Turner et al. 1999; Wang et al. 2010). Qian et al. (2016b) propose that melting of the lithosphere by the upwelling asthenospheric mantle is a potential mechanism governing the genesis of the Late Triassic mafic-intermediate rocks in the Chiang Khong–Lampang–Tak igneous zone. This mechanism may be used to interpret the genesis of the high ε_{Hf} (t) and ε_{Nd} (t) rhyolites along the Chiang Khong–Lampang–Tak igneous zone. Bodet and Schärer (2000) identified five main Proterozoic crustal growth events in the area at around 2.5, 2.3, 1.9, 1.1 and 0.8 Ga. Chiang Khong rhyolite samples were probably the result of partial melting of juvenile mafic lower crust and have Nd model ages of 0.80–0.81 Ga and Hf T_{DM1} of 0.41–0.72 Ga (the average is 0.62 Ga), which may record Neoproterozoic crustal growth in the area.

Conclusions

Geochronological and geochemical data for the Late Triassic rhyolites in the Chiang Khong–Lampang–Tak igneous zone allow us to draw the following conclusions:

1. Zircon U–Pb dating provides an age of 230.7 ± 1.1 Ma for the Chiang Khong rhyolites.
2. The Chiang Khong rhyolites can be classified as I-type rhyolite and are characterized by depleted Hf and Nd isotopic compositions and homogenous mantle-like $\delta^{18}O$ values, suggesting that they originated from partial melting of juvenile mafic lower crust.
3. Late Triassic rhyolites may have formed in a post-collisional tectonic setting related to the upwelling of asthenospheric mantle.

Acknowledgments This work was jointly supported by the National Natural Science Foundation of China (41190073 and 41172202), the China Geological Survey (1212011121256), the National Basic Research Program of China (2014CB440901), "the Fundamental Research Funds for the Central Universities to SYSU" and the State Key Laboratory of Geological Processes and Mineral Resources, China University of Geosciences in Wuhan (MSFGPMR201402). We are grateful to Prof. Wolf-Christian Dullo, Prof. Åke Johansson and another anonymous reviewer for their critical and constructive reviews and comments on this paper.

References

Amelin Y, Lee DC, Halliday AN, Pidgeon RT (1999) Nature of the Earth's earliest crust from hafnium isotopes in single detrital zircons. Nature 399:252–255

Atherton MP, Petford N (1993) Generation of sodium-rich magmas from newly underplated basaltic crust. Nature 362:144–146

Audétat A (2010) Source and evolution of molybdenum in the porphyry Mo (–Nb) deposit at Cave Peak, Texas. J Petrol 51:1739–1760

Barr SM, Charusiri P (2011) Volcanic rocks. In: Ridd MF, Barber AJ, Crow MJ (eds) The geology of Thailand. Geological Society, London, pp 415–439

Barr SM, MacDonald AS, Ounchanum P, Yaowanoiyothin W (2000) Petrochemistry, U–Pb (zircon) age, and paleotectonic setting of the Lampang volcanic belt, northern Thailand. J Geol Soc Lond 157:553–563

Barr SM, Macdonald AS, Ounchanum P, Hamilton MA (2006) Age, tectonic setting and regional implications of the Chiang Khong volcanic suite, northern Thailand. J Geol Soc Lond 163:1037–1046

Barth AP, Wooden JL, Tosdal RM, Morrison J (1995) Crustal contamination in the petrogenesis of a calc-alkalic rock series: Josephine mountain intrusion, California. Geol Soc Am Bull 107:201–212

Bird P (1979) Continental delamination and the Colorado Plateau. J Geophys Res 84:7561–7571

Blichert TJ, Albarède F (1997) The Lu–Hf isotope geochemistry of chondrites and the evolution of the mantle–crust system. Earth Planet Sci Lett 148:243–258

Bodet F, Schärer U (2000) Evolution of the SE-Asian continent from U–Pb and Hf isotopes in single grains of zircon and baddeleyite from large rivers. Geochim Cosmochim Acta 64:2067–2091

Clemens JD, Stevens G, Farina F (2011) The enigmatic sources of I-type granites: the peritectic connexion. Lithos 126:174–181

Cocker JD, Griffin BJ, Muehlenbachs K (1982) Oxygen and carbon isotope evidence for seawater–hydrothermal alteration of the Macquarie Island ophiolite. Earth Planet Sci Lett 61:112–122

Cooke RA, O'Brien PJ (2001) Resolving the relationship between high P–T rocks and gneisses in collisional terrane: an example from the Gföhl gneiss–granulite association in the Moldanubian Zone, Austria. Lithos 58:33–54

Davies JH, von Blanckenburg F (1995) Slab breakoff: a model of lithosphere detachment and its test in the magmatism and deformation of collisional orogens. Earth Planet Sci Lett 129:85–102

Dong GC, Mo XX, Zhao ZD, Zhu DC, Goodman RC, Kong H, Wang S (2013) Zircon U–Pb dating and the petrological and geochemical constraints on Lincang granite in Western Yunnan, China: implications for the closure of the Paleo-Tethys Ocean. J Asian Earth Sci 62:282–294

Eiler JM, Schiano P, Kitchen N, Stolper EM (2000) Oxygen–isotope evidence for recycled crust in the sources of mid–ocean–ridge basalts. Nature 403:530–534

Fan WM, Wang YJ, Zhang YH, Zhang YZ, Jourdan F, Zi JW, Liu HC (2015) Paleotethyan subduction process revealed from Triassic blueschists in the Lancang tectonic belt of Southwest China. Tectonophysics. doi:10.1016/j.tecto.2014.12.021

Feng QL, Chonglakmani C, Helmcke D, Helmcke RI, Liu BP (2005) Correlation of Triassic stratigraphy between the Simao and Lampang-Phrase basins: implications for the tectonopaleogeography of Southeast Asia. J Asian Earth Sci 24:777–785

Gardiner NJ, Searle MP, Morley CK, Whitehouse MP, Spencer CJ, Robb LJ (2015) The closure of Palaeo-Tethys in Eastern Myanmar and Northern Thailand: new insights from zircon U–Pb and Hf isotope data. Gondwana Res. doi:10.1016/j.gr.2015.03.001

Gregory RT, Taylor HP (1981) An oxygen isotope profile in a section of Cretaceous Oceanic Crust, Samail Ophiolite, Oman: evidence for $\delta^{18}O$ buffering of the oceans by deep (>5 km) seawater–hydrothermal circulation at mid-ocean ridges. J Geophys Res 86:2737–2755

Griffin WL, Pearson NJ, Belousova E, Jackson SE, O'Reilly SY, van Achterberg E, Shee SR (2000) The Hf isotope composition of cratonic mantle: lAM–MC–ICPMS analysis of zircon megacrysts in kimberlites. Geochim Cosmochim Acta 64:133–147

Hennig D, Lehmann B, Frei D, Belyatsky B, Zhao XF, Cabral AR, Zeng PS, Zhou MF, Schmidt K (2009) Early Permian seafloor to continental arc magmatism in the eastern Paleo-Tethys: U-Pb age and Nd-Sr isotope data from the southern Lancangjiang zone, Yunnan, China. Lithos 113:408–422

Intasopa SB, Dunn T (1994) Petrology and Sr–Nd isotopic systems of the basalts and rhyolites, Loei, Thailand. J Southeast Asian Earth Sci 9:167–180

Jian P, Liu D, Sun X (2003) SHRIMP dating of Baimaxueshan and Ludian granitoid batholiths, northwestern yunnan province, and its geological implications. Acta Geol Sin 24:337–342

Jungyusuk N, Khositanont S (1992) Volcanic rocks and associated mineralization in Thailand. In: Piancharoen C (ed) Proceedings of the national conference on geologic resources of Thailand: potential for future development. Bangkok, pp 528–532

Kong HL, Dong GC, Mo XX, Zhao ZD, Zhu DC, Wang S, Li R, Wang QL (2012) Petrogenisis of Lincang granites in Sanjiang area of Western Yunnan province: constraints from geochemistry, zircon U–Pb geochronology and Hf isotope. Acta Pet Sin 28:1438–1452

Le Bas MJ, Le Maitre RW, Streckheisen A, Zanettin B (1986) A chemical classification of volcanic rocks based on the total alkali–silica diagram. J Petrol 27:745–750

Leloup PH, Lacassin R, Tapponnier P, Schärer U, Zhong DL, Liu XH, Zhang LS, Ji SC, Trong Trinh P (1995) The Ailao Shan-Red River shear zone (Yunnan, China), Tertiary transform boundary of Indochina. Tectonophysics 251:3–84

Li XH, Li ZX, Zhou HW, Liu Y, Kinny PD (2002) U–Pb zircon geochronology, geochemistry and Nd isotopic study of Neoproterozoic bimodal volcanic rocks in the Kangdian Rift of South China: implications for the initial rifting of Rodinia. Precambrian Res 113:135–154

Li XH, Li WX, Li QL, Wang XC, Liu Y, Yang YH (2010a) Petrogenesis and tectonic significance of the 850 Ma Gangbian alkaline complex in South China: evidence from in situ zircon U–Pb dating, Hf–O isotopes and whole-rock geochemistry. Lithos 114:1–15

Li XH, Long WG, Li QL (2010b) Penglai zircon megacrysts: a potential new working reference material for microbeam determination of Hf–O isotopes and U–Pb age. Geostand Geoanal Res 34:117–134

Li XH, Tang GQ, Gong B, Yang YH, Hou KJ, Hu ZC, Li QL, Liu Y, Li WX (2013) Qinghu zircon: a working reference for microbeam analysis of U–Pb age and Hf and O isotopes. Chin Sci Bull 58:4647–4654

Liu BP, Feng QL, Fang NQ (1991) Tectonic evolution of the Paleo-Tethys in Changning-Menglian belt and adjacent regions, western Yunnan. J China Univ Geosci 2:18–28 **(in Chinese with English abstract)**

Liu HC, Wang YJ, Fan WM, Zi JW, Cai YF, Yang G (2014) Petrogenesis and tectonic implications of Late-Triassic high εNd (t)–εHf (t) granites in the Ailaoshan tectonic zone (SW China). Sci China Earth Sci 57:2181–2194

Ludwig KR (2003) User's manual for Isoplot 3.00: a geochronological toolkit for microsoft excel. Berkeley Geochronology Center, Berkeley, pp 1–70

Luo W, Yin H (1988) Characteristics of the Ludian granite, northwest Yunnan, China. Acta Petrol Sin 2:69–77 **(in Chinese with English abstract)**

Metcalfe I (2002) Permian tectonic framework and palaeogeography of SE Asia. J Asian Earth Sci 20:551–566

Mo XX, Shen SY, Zhu QW (1998) Volcanics–ophiolite and mineralization of middle and southern part in Sanjiang, Southern China. Geological Publishing House, Beijing, pp 1–128 **(in Chinese)**

Panjasawatwong Y (2003) Tectonic setting of the permo-triassic Chiang Khong volcanic rocks, Northern Thailand based on petrochemical characteristics. Gondwana Res 6:743–755

Panjasawatwong Y, Zaw Khin, Chantaramee S, Limtrakun P, Pirarai K (2006) Geochemistry and tectonic setting of the Central Loei volcanic rocks, Pak Chom area, Loei, northeastern Thailand. J Asian Earth Sci 26:77–90

Pearce JA (1996) Sources and settings of granitic rocks. Episodes 19:120–125

Peccerillo A, Barberio MR, Yirgu G, Ayalew D, Barbieri M, Wu TW (2003) Relationships between mafic and peralkaline silicic magmatism in continental rift settings: a petrological, geochemical and isotopic study of the Gedemsa volcano, central Ethiopian rift. J Petrol 44:2003–2032

Peng TP, Wang YJ, Fan WM, Liu DY, Shi YR, Miao LC (2006) SHRIMP zircon U–Pb geochronology of early Mesozoic felsic igneous rocks from the southern Lancangjiang and its tectonic implications. Sci China: Ser D 49:1032–1042

Peng TP, Wang YP, Zhao GC, Fan WM, Peng BX (2008) Arc–like volcanic rocks from the southern Lancangjiang zone, SW China: geochronological and geochemical constraints on their petrogenesis and tectonic implications. Lithos 102:358–373

Peng TP, Wilde SA, Wang Y, Fan W, Peng B (2013) Mid-Triassic felsic igneous rocks from the southern Lancangjiang Zone, SW China: petrogenesis and implications for the evolution of Paleo-Tethys. Lithos 168–169:15–32

Phajuy B (2001) Geochemistry, petrology and tectonic setting of Permo–Triassic mafic volcanic rocks in the northern part of Chiang Khong–Tak volcanic belt. MS Thesis, Chiang Mai University, Chiang Mai

Qian X, Feng QL, Chonglakmani C, Monjai D (2013) Geochemical and geochronological constrains on the Chiang Khong volcanic rocks (northwestern Thailand) and its tectonic implications. Front Earth Sci 7:508–521

Qian X, Feng QL, Yang WQ, Wang YJ, Chonglakmani C, Monjai D (2015) Arc-like volcanic rocks in NW Laos: geochronological and geochemical constraints and their tectonic implications. J Asian Earth Sci 98:342–357

Qian X, Feng QL, Wang YJ, Chonglakmani C, Monjai D (2016a) Geochronological and geochemical constraints on the mafic rocks along the Luang Prabang zone: carboniferous back-arc setting in northwest Laos. Lithos 245:60–75

Qian X, Wang YJ, Feng QL, Zi JW, Zhang YZ, Chonglakmani C (2016b) Petrogenesis and tectonic implication of the Late Triassic post-collisional volcanic rocks in Chiang Khong, NW Thailand. Lithos 245–251:418–431

Rapp RP, Watson EB (1995) Dehydration melting of metabasalt at 8–32 kbar: implications for continental growth and crust-mantle recycling. J Petrol 36:891–931

Roberts MP, Clemens JD (1993) Origin of high-potassium, calc-alkaline, I-type granitoids. Geology 21:825–828

Sisson TW, Ratajeski K, Hankins WB, Glazner AF (2005) Voluminous granitic magmas from common basaltic sources. Contrib Mineral Petrol 148:635–661

Söderlund U, Patchett PJ, Vervoort JD, Isachsen CE (2004) The 176Lu decay constant determined by Lu–Hf and U–Pb isotope systematics of Precambrian mafic intrusions. Earth Planet Sci Lett 219:311–324

Sone M, Metcalfe I (2008) Parallel Tethyan sutures in mainland Southeast Asia: new insights for Paleo-Tethys closure and implications for the Indosinian orogeny. Geoscience 340:166–179

Sone M, Metcalfe I, Chaodumrong P (2012) The Chanthaburi terrane of southeastern Thailand: stratigraphic confirmation as a disrupted segment of the Sukhothai Arc. J Asian Earth Sci 61:16–32

Srichan W, Crawford AJ, Berry RF (2009) Geochemistry and geochronology of Late Triassic volcanic rocks in the Chiang Khong region, northern Thailand. Isl Arc 18:32–51

Sun SS, McDonough WF (1989) Chemical and isotopic systematics of oceanic basalt: implications for mantle composition and processes. In: Saunders AD, Norry MJ (eds) Magmatism in the Ocean Basins, Special Publications, 42. The Geological Society, London, pp 313–345

Sylvester PJ (1998) Post-collisional strongly peraluminous granites. Lithos 45:29–44

Turner SP, Platt JP, George RMM, Kelley SP, Pearson DG, Nowell GM (1999) Magmatism associated with orogenic collapse of the Betic-Alboran domain, SE Spain. J Petrol 40:1011–1036

Ueno K, Hisada K (2001) The Nan–Uttaradit–Sa Kaeo Suture as a main Paleo-Tethyan suture in Thailand: is it real? Gondwana Res 4:804–806

Valley JW, Lackey JS, Cavosie AJ, Clechenko CC, Spicuzza MJ, Basei MAS, Bindeman IN, Ferreira VP, Sial AN, King EM, Peck WH, Sinha AK, Wei CS (2005) 4.4 billion years of crustal maturation: oxygen isotope ratios of magmatic zircon. Contrib Mineral Petrol 150:561–580

von Braun E, Hahn L (1976) Geological map of northern Thailand, sheet 2, Chiang Rai, Scale 1: 250000. Federal Institute for Geosciences and Natural Resources, Stuttgart

Wang YJ, Zhang AM, Fan WM, Peng TP, Zhang FF, Zhang YH, Bi XW (2010) Petrogenesis of late Triassic post-collisional basaltic rocks of the Lancangjiang tectonic zone, southwest China, and tectonic implications for the evolution of the eastern Paleotethys: geochronological and geochemical constraints. Lithos 120:529–546

Wang S, Dong GC, Mo XX, Zhao ZD, Zhu DC, Kong HL, Wang X, Nie F (2012) Petrological and geochemical characteristics, Ar–Ar geochronology study and their tectonic significance of Triassic volcanic rocks in southern Lancangjiang zone. Acta Petrol Sin 28:1148–1162 **(in Chinese with English abstract)**

Wei GJ, Liang XR, Li XH, Liu Y (2002) Precise measurement of Sr isotopic composition of liquid and solid base using (LP) MC–ICPMS. Geochimica 31:295–299

Whalen JB, Currie KL, Chappell BW (1987) A-type granites: geochemical characteristics, discrimination and petrogenesis. Contrib Mineral Petrol 95:407–419

Wright JB (1969) A simple alkalinity ratio and its application to questions of non-orogenic granite genesis. Geol Mag 106:370–384

Wu YB, Zheng YF (2004) Genesis of zircon and its constraints on interpretation of U–Pb age. Chin Sci Bull 49:1554–1569

Wu HR, Boulter CA, Ke B, Stow DAV, Wang Z (1995) The Changning–Menglian suture zone: a segment of the major Cathaysia–Gondwana divide in Southeast Asia. Tectonophysics 242:267–280

Wu FY, Jahn BM, Wilde SA, Lo CH, Yui TF, Lin Q, Ge WC, Sun DY (2003a) Highly fractionated I-type granites in NE China (I): geochronology and petrogenesis. Lithos 66:141–273

Wu FY, Jahn BM, Wilde SA, Lo CH, Yui TF, Lin Q, Ge WC, Sun DY (2003b) Highly fractionated I-type granites in NE China (II): isotopic geochemistry and implications for crustal growth in the Phanerozoic. Lithos 67:191–204

Wu FY, Yang YH, Xie LW, Yang JH, Xu P (2006) Hf isotopic compositions of the standard zircons and baddeleyites used in U–Pb geochronology. Chem Geol 234:105–126

Yuan H, Gao S, Liu XM, Günther D, Wu FY (2004) Accurate U–Pb age and trace element determinations of zircon by laser ablation–inductively coupled plasma–mass spectrometry. Geostand Geoanal Res 28:353–370

Zhang Q, Jin WJ, Wang YL, Li CD, Wang Y, Jia XQ (2006) Ocean lithosphere delamination and the lower crust delamination: the different mechanism and geological implication: comment on the delamination model of lower crust and lithosphere mantle. Acta Petrol Sin 22:2631–2638 **(in Chinese with English abstract)**

Zhang D, Wei J, Fu L, Chen H, Tan J, Li Y, Shi W, Tian N (2015) Formation of the Jurassic Changboshan-Xieniqishan highly fractionated I-type granites, northeastern China: implication for the

partial melting of juvenile crust induced by asthenospheric mantle upwelling. Geol J 50:122–138

Zhao JH, Zhou MF (2009) Melting of newly formed mafic crust for the formation of Neoproterozoic I-type granite in the Hannan region, South China. J Geol 117:54–70

Zhong DL (1998) Paleotethysides in West Yunnan and Sichuan, China. Science Press, Beijing, pp 1–231 **(in Chinese)**

Zhu JJ, Hu RZ, Bi XW, Zhong H, Chen H (2011) Zircon U–Pb ages, Hf–O isotopes and whole-rock Sr–Nd–Pb isotopic geochemistry of granitoids in the Jinshajiang suture zone, SW China: constraints on petrogenesis and tectonic evolution of the Paleo-Tethys Ocean. Lithos 126:248–264

Zi JW, Cawood PA, Fan WM, Wang YJ, Tohver E (2012) Contrasting rift and subduction–related plagiogranites in the Jinshajiang ophiolitic melange, southwest China, and implications for the Paleo-Tethys. Tectonics. doi:10.1029/2011TC002937

Zi JW, Cawood PA, Fan WM, Tohver E, Wang YJ, McCuaig TC, Peng TP (2013) Late Permian-Triassic magmatic evolution in the Jinshajiang orogenic belt, SW China and implications for orogenic processes following closure of the Paleo-Tethys. Am J Sci 313:81–112

Zindler A, Hart SR (1986) Chemical geodynamics. Ann Rev Earth Planet Sci Lett 14:493–571